3-Dimensional Electrical Impedance Spectroscopy for *in situ* Endoluminal Mapping of Metabolically Active Plaques

Parinaz Abiri*[1,2], Yuan Luo*[3,4,], Zi-Yu Huang*[4], Qingyu Cui*[2], Sandra Duarte-Vogel[5], Mehrdad Roustaei[1], Chih-Chiang Chang[1], Xiao Xiao[1], Rene packard[2], Susana Cavallero[2], Ramin Ebrahimi[2], Peyman Benharash[6], Jun Chen[1], Yu-Chong Tai[4], Tzung K. Hsiai[1,2,4†]

Affiliations:

[1] Department of Bioengineering, University of California, Los Angeles, Los Angeles, CA 90095
[2] Division of Cardiology, Department of Medicine, David Geffen School of Medicine, University of California, Los Angeles, Los Angeles, CA 90095
[3] State Key Laboratory of Transducer Technology, Shanghai Institute of Microsystem and Information Technology, Chinese Academy of Sciences, Shanghai, 200050, China; and Center of Materials Science and Optoelectronics Engineering, University of Chinese Academy of Sciences, Beijing, 100049 China
[4] Department of Medical Engineering, California Institute of Technology, Pasadena, CA 91125
[5] Division of Laboratory Animal Medicine, University of California, Los Angeles, Los Angeles, CA 90095
[6] Division of Cardiac Surgery, Department of Surgery, David Geffen School of Medicine, University of California, Los Angeles, Los Angeles, CA 90095

* These authors contributed equally to this work.
† Corresponding Author: THsiai@mednet.ucla.edu.

Supplementary Materials:

List of contents:

SI-1. Partial ligation of carotid arteries in Yucatan mini-pigs

All animals were fed on a high-fat diet containing 4% cholesterol, 20% saturated fat, and 1.5% supplemental choline (Test Diet; Purina, St. Louis, MO) for 2 weeks before surgical ligation of the right carotid arteries. The pigs were anesthetized with intramuscular Tiletamine and Zolazepam, and Isoflurane was given to maintain general anesthesia during the procedure. A 6F introducer sheath was inserted percutaneously via the Seldinger procedure into the right or left femoral artery to monitor blood pressure and to provide access for angiography. Bupivacaine was subcutaneously injected in the ventral neck along the path of the incision site. A midline skin incision was placed at the neck. Both right and left common carotid arteries were dissected approximately 5 cm in length, but the right common carotid artery was tied off with a suture (Ethicon, Cornelia, Ga) around a spacer (approximately 1.3 mm in diameter) positioned on the external surface of the artery. The spacer was subsequently pulled out, leaving a 50-70% stenosis. Postoperative CT angiography was performed to monitor the degree of surgical stenosis.

To deploy the microelectrode array for 3-D EIS measurement, the animals were anesthetized as described above (**SI-1**). Bupivacaine was subcutaneously injected in the ventral neck along the path of the incision site. A midline skin incision was placed at the neck. The common carotid arteries were dissected and a surgical cut-down was performed to directly introduce the sheath and device into the carotid artery at the site of stenosis in the right carotid artery and at the approximate mirror location in the left carotid artery.

Supplementary Figure for Movat staining.

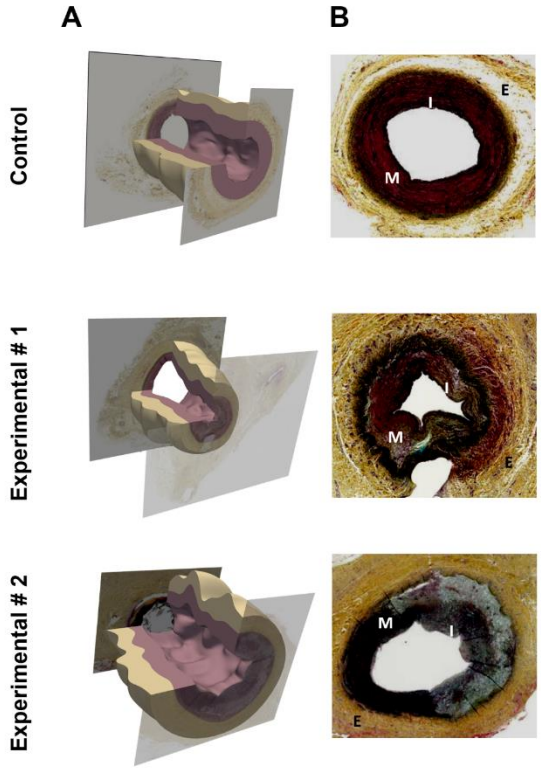

Fig. SI-1. Histological Mapping of Carotid Arteries. (A) The 3-D histological reconstruction recapitulates the endoluminal topology from 11 cross-sections of a segment (4 mm) of carotid arteries. (B) The representative Movat staining for connective tissue was compared between the left and right carotid arteries. I: tunica intima; M: tunica media; E: tunica externa.

SI-2. Deviation between the computational and experimental impedance

From each electrode position (z, θ), we calculated the summation of the square of the differences between the experimental and simulated EIS from the same pair of electrodes. The electrode position resulting the largest reciprocal of the deviation, which is the square root of the summation, is defined as the best fit scenario. The best fit electrode positions are circled in green in the 3-D deviation plots (**Fig. SI-2**).

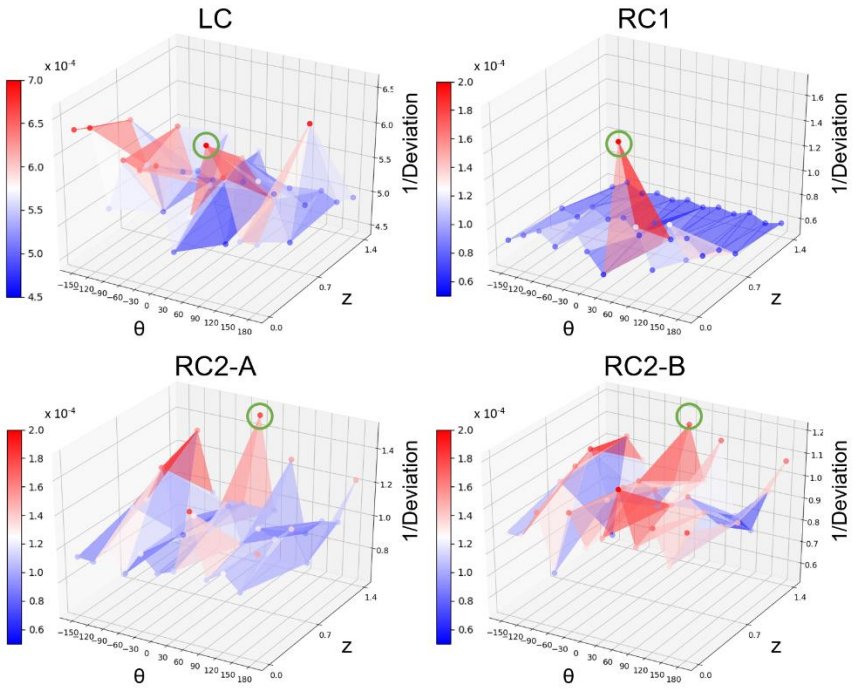

Fig. SI-2: Deviation plots. Total 36 electrode placements were tested in the simulation models. The deviations between the simulated impedance and experimental impedance at 10 kHz were calculated and the best fit scenario of electrode position is highlighted in the green circle.

SI-3. Comparison between EIS impedance measurement with the finite element model

From each carotid artery sample, we created a 3-D model and scanned through possible electrode positions with a different combination of z and θ. 15-permutation impedance values were calculated for each combination, and computational EIS profiles were compared with the measured EIS to identify the best fit scenarios. Scatter plots of the 15-permutation impedance from the measured EIS and representative computation model (simulation) are presented with the best fit combination of z and θ as highlighted in light blue (**Fig. SI-3**).

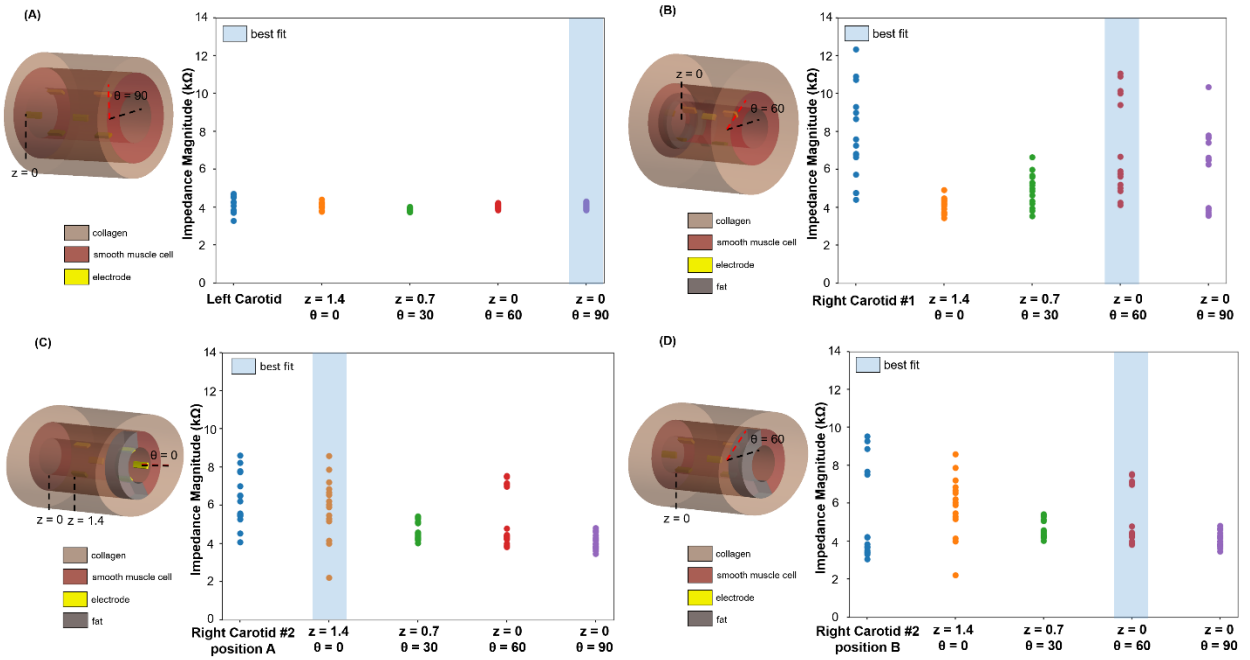

Fig. SI-3: Computation Models. Comparisons with the simplified 3-D schematic indicate the position of the electrodes in the endolumen where the computational impedance values are overlapping with the experimental EIS. Experimental impedance at 10 kHz is plotted alongside the modeling results at the given z and θ values, and the combination with the best fit was highlighted. Computational EIS are compared among (A) LCA, (B) RCA1, (C) RCA2 position A, and (D) RCA2 position B.

SI-4. Comparison of impedance measurement before and after electroplating

The flexible electrodes (either before or after electroplating) were submerged in a large container of saline solution (0.9% wt NaCl). The geometric effect was considered negligible under these settings. The impedance spectra were measured using Gamry G 300 with 50 mV, and the frequency ranged from 100 Hz to 300 kHz. The electroplating of Pt Black resulted in a low contact impedance for the electrodes, as evidenced by the significantly flattening in the EIS curve beyond 1 kHz. Therefore, we validated the selection of 10 kHz for the EIS analyses and computational modeling.

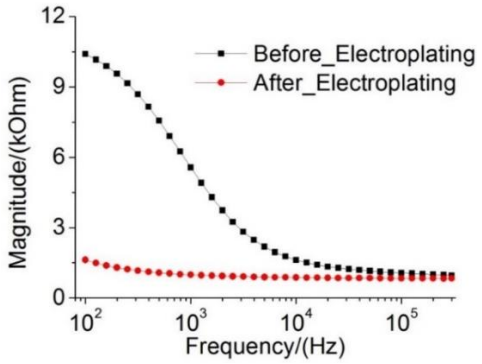

Fig. SI-4: **Electrochemical impedance spectra.** A comparison between before and after electroplating demonstrated a significant decrease in contact impedance.

SI-5. Reconstruction of conductivity mapping from the impedance data

Our computational model was composed of the arterial wall that was represented by 576 elements (**Figure SI-5Bi**), and the annular collagen layer by 288 elements (**Figure SI-5Bii**). The initial conductivities of arterial wall elements were derived from the EIS measurements. The collagen layer was assigned with a large element size and a uniform conductivity. We varied the conductivity distribution to a direction that optimally reproduced the 15 permutations for the impedance measurements. To this end, we used the "genetic algorithm" so that all elements "evolved" to reach the final mapping results. The implementation was as follows: the conductivity value from each of the 864 elements was considered as an 864×1 vector. We generated a solution candidate pool (100) by adding a Gaussian-distributed noise to this initial 864×1 vector, $\vec{C}_1, \vec{C}_2, \ldots \vec{C}_{100}$. For each candidate, we calculated the 15 impedance values by solving the Laplace equation:

$$Z_{12,\mathrm{sim}}, Z_{13,\mathrm{sim}}, Z_{14,\mathrm{sim}}, \ldots Z_{56,\mathrm{sim}} \quad (1)$$

We defined our fitness function as follows:

$$f = \sqrt{(Z_{12,\mathrm{measured}} - Z_{12,\mathrm{sim}})^2 + (Z_{13,\mathrm{measured}} - Z_{13,\mathrm{sim}})^2 + \cdots (Z_{56,\mathrm{measured}} - Z_{56,\mathrm{sim}}} \quad (2)$$

The "genetic algorithm" was implemented by the following steps:

i. Calculate the fitness function for all of the solution candidates in the pool.

ii. Rank the candidates according to their fitness function from small to large values.

iii. Identify the top-10 candidates from the pool: $\vec{C}_1^*, \vec{C}_2^*, \ldots \vec{C}_{10}^*$.

iv. Generate a new pool of 90 candidates as follows:

$$\vec{C}_i^* = \sum_{k=1}^{10} (\sigma \lambda_k \vec{C}_k^* + (1-\sigma)\,\lambda_k \frac{\sum_1^{10} \vec{C}_k^*}{10}), i = 11,12, \ldots 100, \quad (3)$$

where $\sigma = 1.3$ is a factor to moderate the boundaries of the candidate space obtained from the above equation, and $\sum_1^{10} \lambda_k = 1$ (*50*).

Steps i-iv were repeated until the minimum fitness function reaches the predefined target, and the solution candidate $\vec{C}_1^{final}$ was used to assign to the conductivity distribution to generate the final EIT mapping (see **Figure 4**). We excluded the outmost layer as the calculated conductivity distribution was fairly homogeneous since the major heterogeneity resided in the inner layer (576 elements).

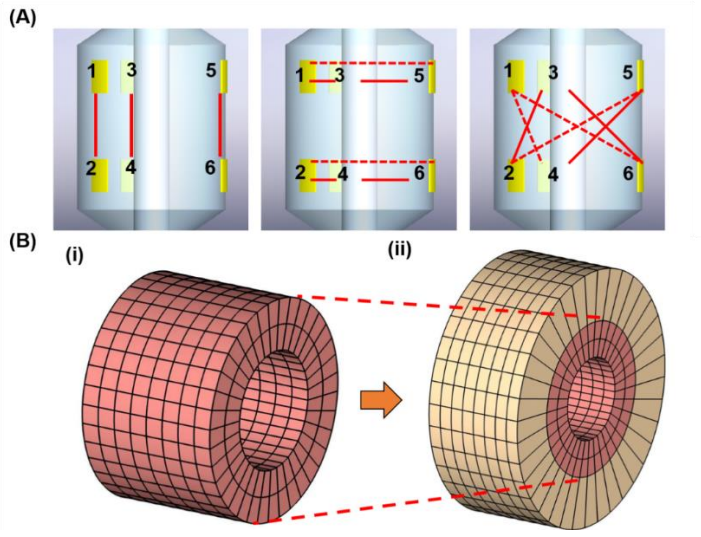

Fig. SI-5: Finite element model for reconstructing the conductivity maps. (A) The configuration of the 6-point electrodes (EIS sensor) generates 15 permutations. (B-i) 576-element mapping scheme represents the inner smooth muscle layer. (B-ii) 864-element mapping scheme includes the collagen layer (yellow).

SI-6. Histology-based 3-D FEM modeling

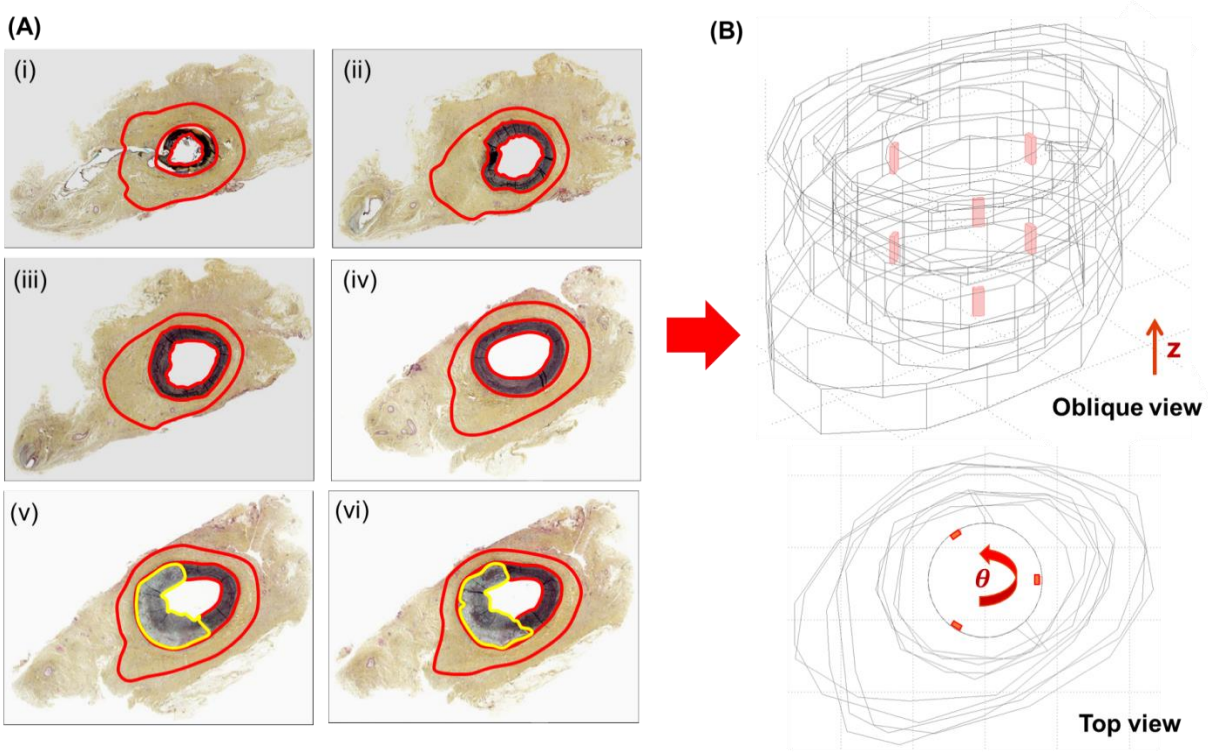

Fig. SI-6: Finite Element Model for 3-D histology and computational modeling. (A) Representative histological cross-sections from the right carotid artery (RC2) were demarcated by the Movat staining for connective tissue, the boundaries for collagen, smooth muscle, and the lipid component. (B) These demarcations from the histological slices allowed for reconstructing a 3-D model. The positions of the electrodes (red) were defined by the z and θ coordinates.

Table I. Tissue properties used for the computational model (57)

	Collagen layer	Smooth muscle cell layer	Fat tissue
$\boldsymbol{\sigma}$ $(\boldsymbol{S/m})$	0.174	0.307	0.042
$\boldsymbol{\varepsilon}$	32000	149000	193000